Lithos 320–321 (2018) 144–154

Contents lists available at ScienceDirect

Lithos

journal homepage: www.elsevier.com/locate/lithos

Spongy texture in mantle clinopyroxene records decompression-induced melting

Shaokui Pan [a], Jianping Zheng [b,*], Zuowei Yin [a,*], W.L. Griffin [c], Mingzhe Xia [d], Abing Lin [b], Hui Zhang [b]

[a] Gemological institute, China University of Geosciences, Wuhan 430074, China
[b] State Key Laboratory of Geological Processes and Mineral Resources, China University of Geosciences, Wuhan 430074, China
[c] ARC Centre of Excellence for Core to Crust Fluid Systems and GEMOC, Department of Earth and Planetary Sciences, Macquarie University, NSW 2109, Australia
[d] The school of earth science and resources, Chang'an University, Xi'an 710054, China

ARTICLE INFO

Article history:
Received 7 October 2017
Accepted 27 August 2018
Available online 30 August 2018

Keywords:
Mantle clinopyroxene
Spongy texture
Decompression-induced melting

ABSTRACT

Spongy texture in clinopyroxene is found in mantle xenolith suites worldwide while its origin commonly is unclear. Detailed petrologic observations and major- and trace-element analysis were conducted on peridotite xenoliths with spongy clinopyroxene, from the central part of the Great Xing'an Range, in the eastern part of the Central Asian Orogenic Belt, to investigate the origin of the texture. Spongy texture mainly occurs as rims of variable thickness on clean cores and occasionally extends into the inner parts of clinopyroxene or even totally covers the whole grain; there is no obvious relationship between the thickness of the rims and their proximity to the host basalt. The boundaries between spongy-textured clinopyroxenes and surrounding minerals are sharp. Spongy domains consist of secondary clinopyroxenes, glasses, vugs and traces of olivine. Relative to the primary ones, clinopyroxenes in spongy domains have low Na_2O, Al_2O_3 and Al^{VI}/Al^{IV}, and high CaO, $Mg^{\#}$ and $Cr^{\#}$. The estimated pressures of spongy domains are 0.34–0.95 Gpa, significantly lower than those of primary peridotite phases (2.10–2.44 Gpa). Glasses in spongy domains are rich in Na_2O and Al_2O_3 and depleted in MgO and FeO, containing a small amount of K_2O. Some glasses have low $Mg^{\#}$ (down to 43.9), and are not in equilibrium with associated clinopyroxenes and olivines. Based on these observations, we suggest that the spongy texture in the studied peridotites was recently formed by decompression-induced low-degree partial melting. By comparing our petrological and chemical data with those of previous studies, textural and chemical criteria are developed to differentiate various possible origins of spongy texture in mantle clinopyroxene.

1. Introduction

Peridotite xenoliths are an essential source of information about physicochemical properties and evolution of the deep lithosphere from which they were derived (Griffin et al., 1998; Zheng et al., 2007; Zheng. 2009; Tang et al., 2013a). Spongy texture, also called sieved texture (Nelson and Montana 1992; Shaw et al., 2006; Shaw and Dingwell 2008), is common in many mantle xenolith suites in the world, such as the Western Qinling (Su et al., 2011), NW Syria (Ma et al., 2015), Northern Tanzania (Dawson 2002), Hessian Depression (Carpenter et al. 2002), Kenya Rift (Kaeser et al., 2007) and Dariganga lava plateau (Ionov et al., 1994). The texture is frequently glass-bearing and characterized by porous rims or coronae of variable thickness on host minerals in mantle peridotite (mainly on clinopyroxene and spinel, occasionally on orthopyroxene and olivine; Streck 2008).

During the past decades, the origin of spongy texture in mantle clinopyroxene has been the subject of some controversy. Some authors have attributed spongy texture to metasomatism by fluid/melt penetration before entrainment in the host magma (Bonadiman et al., 2005, 2008; Carpenter et al., 2002; Ionov et al., 1994; Liang and Elthon 1990). In these cases, melt pockets, interstitial glasses or modal metasomatic minerals were observed with the occurrence of spongy-textured clinopyroxene (Bonadiman et al., 2005; Ionov et al., 1994, 2005). Glasses associated with spongy texture have high $Na_2O + K_2O$ (up 15.5 wt%), but low Na_2O/K_2O (<1), CaO (<3 wt%), MgO (<1.63 wt%) and FeO (<1.44 wt%; Bonadiman et al., 2005). In contrast, other authors have argued that interaction between primary orthopyroxene in peridotite xenolith and host magma during transport could produce a Si- and alkali-rich melt, which causes the incongruent dissolution of clinopyroxene and finally results in the formation of spongy texture (Shaw et al., 2006; Shaw and Dingwell 2008). Spongy-textured clinopyroxene, as well as reacted orthopyroxene, are particularly concentrated near contacts with the host magma (Shaw et al., 2006, Shaw and Dingwell 2008). Spongy clinopyroxenes have higher Ca and Cr and lower Na and Al contents, compared with the primary ones

* Corresponding authors.
E-mail addresses: jpzheng@cug.edu.cn (J. Zheng), yinzuowei@cug.edu.cn (Z. Yin).

https://doi.org/10.1016/j.lithos.2018.08.035
0024-4937/

(Shaw et al., 2006, Shaw and Dingwell 2008). Glasses within spongy domain have high CaO (up to 20 wt%), MgO (up to 15.7 wt%) and $Mg^{\#}$ (78.4–91.4; Shaw et al., 2006, Shaw and Dingwell 2008). Recently, Su et al., (2011) presented petrographical and chemical data on spongy-textured clinopyroxene in peridotites from the West Qinling area. In that study, spongy rims on clinopyroxene are enriched in Ca and depleted in Na and Al. More importantly, Al^{IV}/Al^{VI} of spongy rims is higher than that of intact cores. The authors argued that spongy texture in clinopyroxene developed from decompression-induced partial melting (Su et al., 2011). However, no chemical composition of associated glass was reported.

It thus appears that the origin of spongy texture in mantle clinopyroxene could be related to different processes. Correctly understanding the origin of spongy textures in peridotite minerals is important to reveal the processes operating in the upper mantle and avoid misinterpretations of the mineralogy and chemical compositions of the mantle imposed by post-entrainment lava-xenolith interaction (Ma et al., 2015; Shaw et al., 2006; Su et al., 2011). Therefore, it is necessary to identify criteria to differentiate the origins of these similar spongy textures in mantle clinopyroxene.

Cenozoic basalts are widely distributed in NE China (Fig. 1a), and contain abundant peridotite xenoliths. Previous studies on these xenoliths mainly focused on their formation ages and geochemical characteristics, and discussed the nature and evolution of the lithospheric mantle beneath NE China (Pan et al., 2013, 2015; Wu et al., 2003; Xu et al., 1998; Yu et al., 2009; Zhang et al., 2000, 2011, 2012; Zhou et al., 2007, 2009). Spongy-textured clinopyroxenes in peridotites were recognized in some locations such as Aershan, Shuagliao and Yitong (Fig. 1a; Yu et al. 2007; Zhou et al., 2009; Liu et al., 2014), but little attention was paid to them. In this study, we present detailed petrological and major- and trace-element data on peridotite xenoliths with spongy textures, from the central part of the Great Xing'an Range, in the eastern part of the Central Asian Orogenic Belt. These data allow us to investigate the origin of spongy texture and further develop textural and chemical criteria to differentiate various origins of spongy texture in mantle clinopyroxene, through comparison of our petrological observations and chemical data with those in previous studies.

2. Geological background

The Central Asian Orogenic Belt (called the Altaids in some references), which links the Siberia Craton to the north and the North China Craton to the south, is one of the largest Phanerozoic accretionary orogenic belts on Earth (Sengör and Burtman 1993; Jahn et al., 2000; Kröner et al., 2007; Windley et al., 2007; Wilhem et al., 2012). Tectonically, the Great Xing'an Range is located in the eastern part of the orogen (Fig. 1a). During the Paleozoic, the region was controlled by the Paleo-Asian Ocean tectonic regime and characterized by the amalgamation of several terranes (Wu et al., 2002, 2011; Xiao et al., 2003; Xu et al., 2013). Subsequently, since early Mesozoic, this region has been strongly overprinted by subduction of the Paleo-Pacific and Mongol-Okhotsk Oceans (Wang et al., 2006; Xu et al., 2013; Pan et al., 2014;

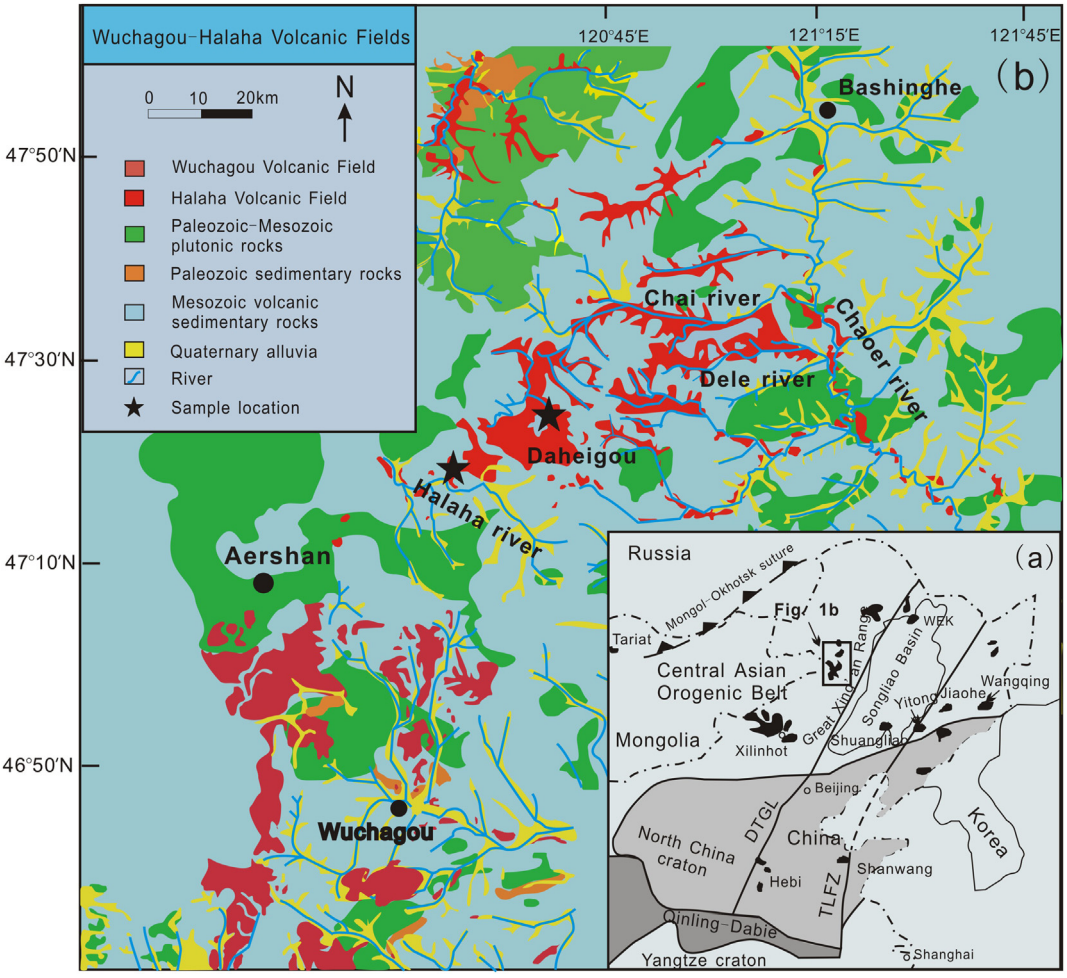

Fig. 1. (a) Tectonic framework of eastern China and the location of the studied area (modified after Xu et al. 2004). (b) Sketch map shows distributions of the Wuchagou and Halaha volcanic field (host lava) and the sample locations (modified after Ho et al., 1991). WEK, Wudalianchi-Erkeshan-Keluo; DTGL, Daxing'anling-Taihangshan gravity lineament; TLFZ, Tanlu translithosperic fault zone.

Table 1
Microstructure and mineral mode of the Aershan peridotite xenoliths, NE China.

Sample	Rock	Ol-Mg#	Microstructure	Modes (wt%)				
				Ol	Opx	Cpx	Sp	Symplectite
AS03	lherzolite	90.3	porphyroclastic	66	25	6		3
AS04	lherzolite	90.4	porphyroclastic	72	18	7	3	
AS06	lherzolite	88.9	protogranular	58	26	6		10
HLH10	lherzolite	90.1	porphyroclastic	65	20	11		4
DHG04	harzburgite	90.1	porphyroclastic	69	23	5		3
DHG10	lherzolite	89.9	protogranular	63	22	14		1
DHG13	harzburgite	90.9	porphyroclastic	73	22	4	1	

Mineral modes of samples are determined by point counting. Ol, olivine; Opx, orthopyroxene; Cpx, clinopyroxene; Sp, spinel.

Tang et al., 2014). The basement of the range is composed of Paleozoic to Mesozoic strata, including low-grade metamorphosed volcano-sedimentary associations, limestones and clastic rocks, which are intruded by voluminous volcanic rocks and granitoids (Ge et al., 2005; Wu et al., 2001, 2011; Zhang et al., 2010). The formation ages of some previously assumed Precambrian metamorphic complexes are still controversial (Ge et al., 2011; Miao et al., 2004; Shi et al., 2003; Sun et al., 2013a). Recently, Paleoproterozoic (1741–1854 Ma) granitic gneisses and Neoproterozoic (737–851 Ma) granitoids were recognized in the northern part of the Great Xing'an Range (Sun et al., 2013b; Tang et al., 2013b).

The Cenozoic volcanic field in the central part of the Great Xing'an Range can be divided into two domains, defined as the Wuchagou volcanic field in the south and the Halaha volcanic field in the north (Fig. 1b). The latter contains abundant peridotite xenoliths, which are rarely found in the former. The Halaha volcanic rocks are alkali basalts and accumulated mainly above the valleys of local rivers, forming a low lava platform. The alkali basalts, with K—Ar ages of 2.0–0.2 Ma, represent the melting products of convective mantle (Ho et al., 2013). The studied peridotites were collected from the valley of the Halaha River, near the city of Aershan (Fig. 1b).

3. Petrography

The studied xenoliths are fresh, rounded to sub-angular but small, predominantly <5 cm in diameter. All the peridotites are anhydrous and contain no metasomatic phases (e.g. amphibole, mica or apatite). The modal compositions of these peridotites have been determined by point-counting with >500 points in each thin section. A summary of their textures and mineral assemblages is given in Table 1.

Spongy-textured clinopyroxene grains occur widely and are randomly distributed across the thin sections. They do not show preferential development (i.e. thicker spongy rims) toward the contact between the peridotite and host basalt (Fig. 2). Most spongy-textured clinopyroxenes are composed of clean cores and spongy rims with thickness from 20 to 250 μm (Fig. 3a). Occasionally, spongy domains extend into the inner part of the host clinopyroxene (Fig. 3b) or even totally cover the whole grain. It appears that the development of spongy domains is not controlled by cracks across clinopyroxene (Fig. 3c). The boundaries between spongy-textured clinopyroxenes and surrounding mineral grains are sharp. Spongy-textured clinopyroxenes also display well-defined contacts between the spongy rims and the intact cores, and the latter do not show any zoning pattern in back-scattered electron images (Fig. 3d and e).

Spongy domains are mainly composed of secondary clinopyroxenes, glasses and vugs. Clinopyroxene in the spongy part is brighter than the corresponding intact core in back-scattered electron images (Fig. 3a, d and e). They share optical continuity under cross-polarized light (Fig. 3f). Glasses are dark grey. Vugs are always empty and vary from round to worm-like shapes, or even form net-channels (Fig. 3a, c, d and e). Traces of olivine (<3 vol% of the spongy domain), are anhedral to euhedral and accompanied by glasses or vugs (Fig. 3d and e), and are ubiquitous in spongy domains of most samples. Samples DHG13 and AS04 are spinel-bearing harzburgite and lherzolite, respectively. Other samples (AS03, AS06, DHG04, DHG10 and HLH10) contain symplectite (Fig. 4a) which consists of tiny spinels, orthopyroxenes and quenched glasses (Fig. 4b). The relationship between symplectite and spongy-textured clinopyroxene is hard to investigate because

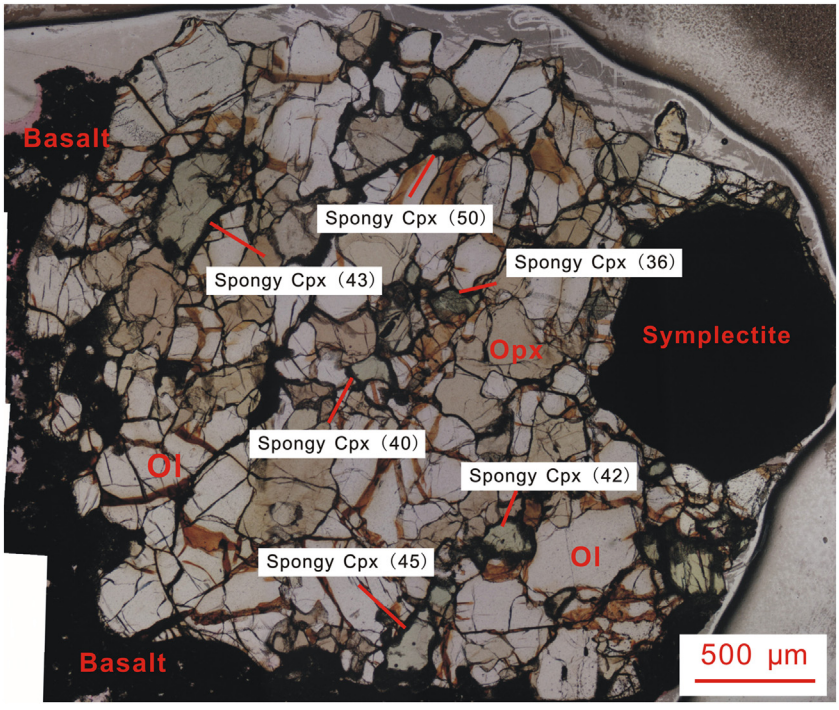

Fig. 2. Scanned thin section of xenolith (sample AS06). Ol: olivine; Opx: orthopyroxene; Cpx: clinopyroxene. Numbers in brackets are average thickness (nm) for each spongy rim on clinopyroxene.

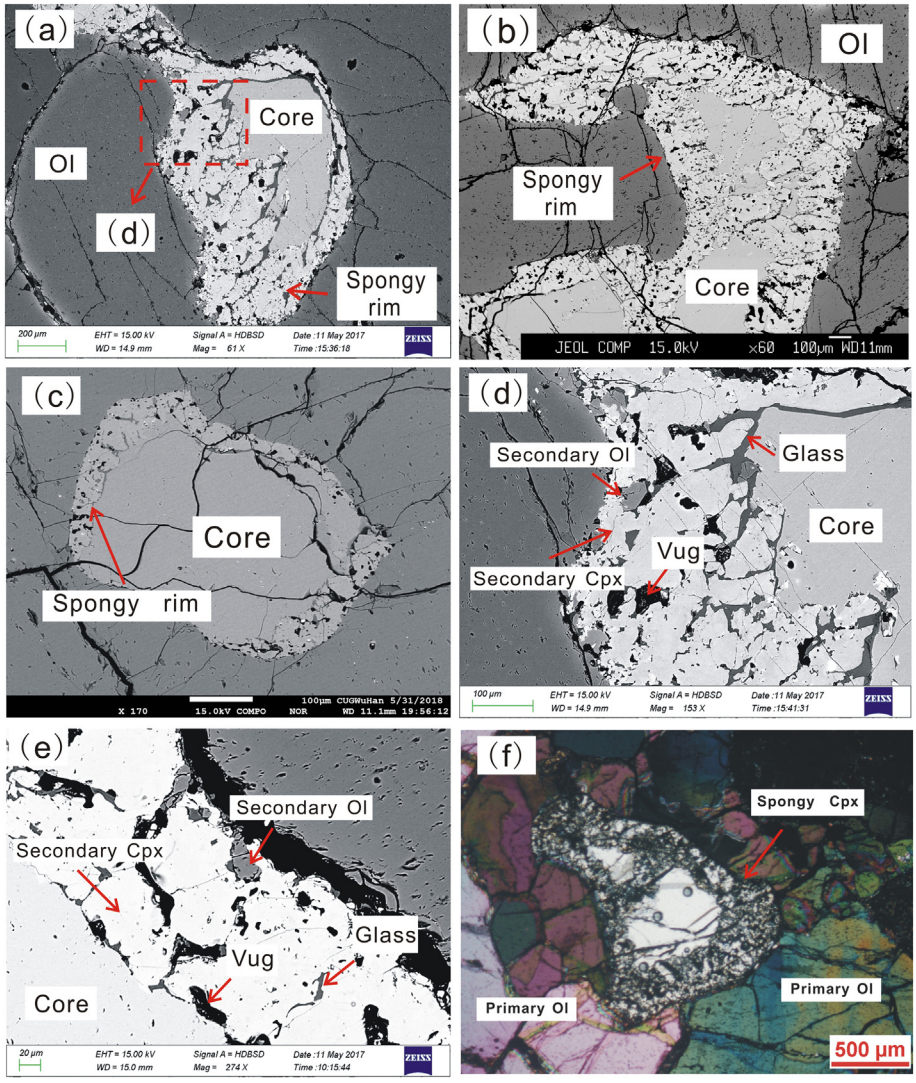

Fig. 3. BSE micrographs (a, b, c, d and e) and photomicrograph (f) of spongy-textured clinopyroxene in the Aershan peridotites. (a) Spongy rim of clinopyroxene in AS04 showing variable thickness. (b) Spongy domain extends into the inner part of host clinopyroxene in DHG04. (c) Cracks crosscut a clinopyroxene grain in DHG04. (d) and (e) Spongy domain consists of secondary olivines, clinopyroxenes, glasses and variable-shaped vugs. (f) A spongy-textured clinopyroxene grain in DHG04 under cross-polarized light. Ol: olivine; Cpx: clinopyroxene.

they are not connected with each other. The inner parts of some symplectites are composed of ultra-fine mineral grains (<1 μm).

4. Analytical methods

Major-element analyses of primary minerals and different materials in spongy domains were carried out at the State Key Laboratory of Geological Processes and Mineral Resources, China University of Geosciences (Wuhan), with a JEOL JXA-8100 Electron Probe Micro Analyzer equipped with four wavelength-dispersive spectrometers (WDS). The samples were coated with a thin conductive carbon film prior to analysis. The precautions suggested by Zhang and Yang (2016) were used to minimize the difference of carbon film thickness between samples and obtain an approximately uniform coating ca. 20 nm thick.

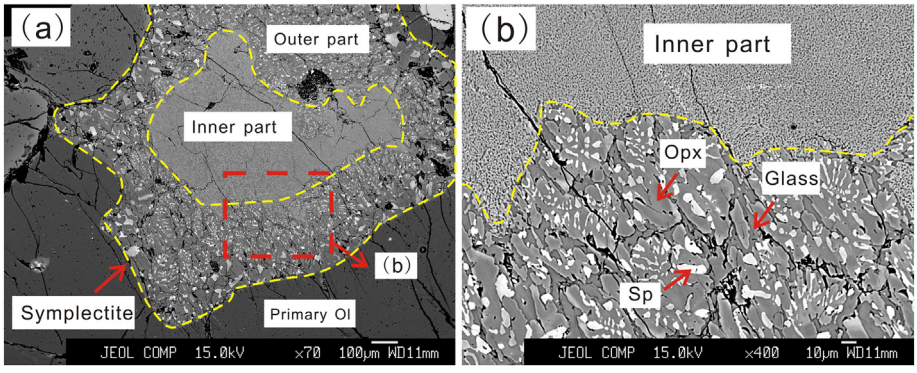

Fig. 4. (a) BSE micrograph of a symplectite in DHG04. (b) Enlarged image of the rectangle in (a), showing the symplectite consists of Opx, Sp and glass. Ol: olivine; Opx: orthopyroxene; Sp: spinel.

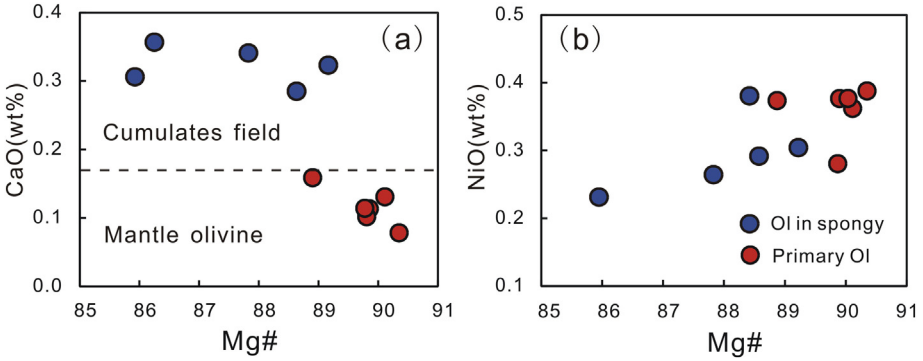

Fig. 5. Plots of $Mg^{\#}$ vs (a) CaO and (b) NiO in primary olivines and secondary ones in spongy area. The compositional boundary between mantle olivine and cumulate olivine is from Thompson and Gibson (2000).

During the analysis, an accelerating voltage of 15 kV, a beam current of 20 nA and a 5 μm spot size were used to analyze minerals. Data were corrected on-line using a modified ZAF (atomic number, absorption, fluorescence) correction procedure. The peak counting time was 10 s for Na, Mg, Al, Si, K, Ca, Fe, Cr, Ni and 20 s for Ti and Mn. The background counting time was one-half of the peak counting time on the high- and low-energy background positions. The following standards were used: Sanidine (K), Pyrope Garnet (Fe, Al), Diopsode (Ca, Mg), Jadeite (Na), Rhodonite (Mn), Olivine (Si), Rutile (Ti), Chromium oxide (Cr).

Trace-element analyses of primary clinopyroxenes and orthopyroxenes were obtained by LA-ICP-MS at the State Key Laboratory of Geological Processes and Mineral Resources, China University of Geosciences, Wuhan. Laser sampling was performed using a GeoLas2005 with laser beam diameter of 44 μm. The ICPMS is an Agilent 7700. Each analysis incorporated a background acquisition of approximately 20–30 s (gas blank) followed by 50 s data acquisition from the sample. The NIST 610 glass and the USGS glasses were used as external standards. No internal standard was applied for correction. Additional descriptions of instrument operating conditions, calibration values, detection limits, and error analysis for the laser microprobe are reported by Liu et al., (2008).

5. Analytical results

5.1. Major-element compositions

5.1.1. Primary minerals

The primary minerals are homogeneous, based on several core and rim analyses in each sample. Their major-element compositions are listed in Appendix 1.

The primary olivine in the studied peridotites has high NiO and low CaO contents (Fig. 5). Its $Mg^{\#}$ varies from 88.9 to 90.9 (Fig. 5). The Al_2O_3 contents of orthopyroxene range from 3.99 to 5.47 wt% and broadly decrease with increasing $Mg^{\#}$. Spinel only occurs in samples DHG13 and AS04, with $Cr^{\#}$ of 26.5–41.8 and $Mg^{\#}$ of 67.0–69.3. All primary clinopyroxenes are Cr-diopside with Cr_2O_3 contents of 0.98–1.60 wt%, displaying a negative correlation of $Mg^{\#}$ vs Al_2O_3 but a positive correlation of $Mg^{\#}$ vs CaO (Fig. 6).

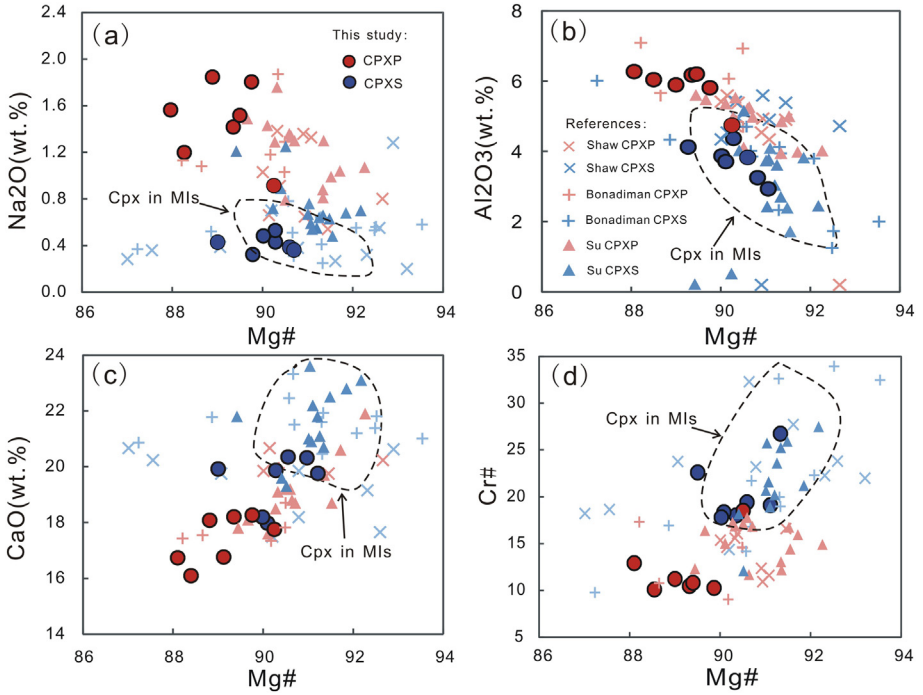

Fig. 6. Plots of $Mg^{\#}$ vs Na_2O (a), Al_2O_3 (b), CaO (c) and $Cr^{\#}$ (d) in primary clinopyroxenes and secondary ones in spongy domain. CPXP: primary clinopyroxene; CPXS: secondary clinopyroxene in spongy domain; Cpx in MIs: clinopyroxene in melt inclusions. Data sources: Shaw CPXP and Shaw CPXS are from Shaw et al. (2006) and Shaw and Dingwell. (2008); Bonadiman CPXP and Bonadiman CPXS are from Bonadiman et al. (2005); Su CPXP and Su CPXS are from Su et al. (2011); Cpx in MIs are from Ionov et al. (2011) and Bénard et al. (2016).

Table 2
Electron microprobe analyses (wt%) of materials in spongy domain of clinopyroxene of the Aershan peridotites.

Sample	AS03			AS04		AS06			HLH10	
	Cpx	Glass	Ol	Cpx	Glass	Cpx	Glass	Ol	Cpx	Glass
Number	10	6	3	11	5	10	5	3	10	5
Na_2O	0.42	5.02	0.02	0.50	5.46	0.39	6.07	0.03	0.39	5.14
K_2O	0.01	0.38	b.d.	0.01	0.52	0.01	0.64	0.00	0.00	0.57
FeO	3.09	0.48	10.20	3.31	0.44	3.58	0.48	11.75	3.33	0.76
MgO	17.60	0.27	46.92	17.25	0.27	16.99	0.21	47.11	17.85	0.60
CaO	20.20	11.05	0.32	19.62	10.01	19.65	9.28	0.35	20.31	10.66
Al_2O_3	3.20	27.16	0.05	4.25	26.44	4.09	26.41	0.07	3.82	27.30
SiO_2	52.59	53.94	40.81	52.05	55.62	51.45	56.71	39.42	51.94	54.48
Cr_2O_3	1.14	0.06	0.07	1.41	0.05	1.80	0.06	0.19	1.39	0.02
TiO_2	0.43	0.10	0.01	0.62	0.19	0.56	0.15	0.03	0.43	0.12
MnO	0.05	0.04	0.31	0.07	0.02	0.07	0.01	0.27	0.09	0.03
NiO	0.06	0.04	0.15	0.10	0.05	0.09	0.00	0.13	0.03	0.01
Total	98.79	98.53	98.84	99.18	99.08	98.69	100.01	99.34	99.58	99.69
$Mg^{\#}$	91.1	50.4	89.2	90.4	52.1	89.5	43.8	87.8	90.6	58.8
$Cr^{\#}$	19.1			18.0		22.6			19.4	
^{IV}Al	0.05			0.09		0.10			0.09	
^{VI}Al	0.09			0.09		0.08			0.08	
$^{VI}Al/^{IV}Al$	1.62			0.95		0.78			0.84	

Sample	HLH10	DHG04			DHG10			DHG13	
	Ol	Cpx	Glass	Ol	Cpx	Glass	Ol	Cpx	Glass
Number	3	12	7	8	11	6	4	12	3
Na_2O	0.02	0.47	5.09	0.03	0.35	4.50	0.03	0.32	4.92
K_2O	0.00	0.01	0.22	0.01	0.01	0.17	b.d.	0.01	0.47
FeO	13.44	3.84	0.57	10.81	3.71	0.66	10.92	3.12	0.44
MgO	45.50	19.41	0.42	46.56	18.61	0.52	46.56	18.27	0.19
CaO	0.31	17.79	10.89	0.28	18.14	11.90	0.27	19.62	11.02
Al_2O_3	0.03	3.88	27.07	0.11	3.96	27.72	0.04	2.98	27.59
SiO_2	39.86	51.99	54.91	40.87	52.50	53.95	40.82	52.97	54.27
Cr_2O_3	0.09	1.32	0.05	0.09	1.29	0.04	0.04	1.64	0.00
TiO_2	0.02	0.42	0.09	0.02	0.36	0.09	0.02	0.35	0.16
MnO	0.24	0.09	0.04	0.30	0.08	0.03	0.38	0.08	0.00
NiO	0.16	0.10	0.05	0.18	0.09	0.04	0.16	0.09	0.07
Total	99.67	99.33	99.40	99.26	99.10	99.61	99.22	99.45	99.13
$Mg^{\#}$	85.9	90.1	56.8	88.6	90.0	58.5	88.5	91.3	44.0
$Cr^{\#}$		18.3			17.8			26.7	
^{IV}Al		0.11			0.08			0.04	
^{VI}Al		0.05			0.09			0.08	
$^{VI}Al/^{IV}Al$		0.47			1.07			1.88	

Ol: olivine; Opx: orthopyroxene; Cpx: clinopyroxene; Sp: spinel; b.d.: below detection limit.

5.1.2. Spongy domains in clinopyroxene

Major-element compositions of different materials (clinopyroxene, glass and olivine) in the spongy domain of clinopyroxene are given in Table 2. Relative to the primary one, secondary olivine in spongy domains has apparently low $Mg^{\#}$ and NiO but high CaO (Fig. 5). Compared with the primary one, secondary clinopyroxene in spongy domains has obviously low Al_2O_3 and Na_2O but high CaO (Figs. 6 and 7). The SiO_2 and TiO_2 concentrations are similar and do not show systematic differences. Glasses in spongy domains show a narrow range in Al_2O_3 (26.4–27.7 wt%), CaO (9.3–11.9 wt%) and SiO_2 (53.9–56.7 wt%). It is poor in MgO (0.19–0.52 wt%), FeO (0.44–0.76 wt%) and TiO_2 (0.09–0.19 wt%) but rich in Na_2O (4.50–6.07 wt%), with a small amount of K_2O (0.17–0.64 wt%). The $Mg^{\#}$ of glass is low and varies from 43.9 to 58.8.

5.2. Trace-element compositions

Trace-element compositions of primary clinopyroxene and orthopyroxene are listed in Appendix 2. Chondrite-normalized REE patterns for primary clinopyroxene are convex-upward, with peaks at Sm, Nd and Eu (Fig. 8a). The extended trace-element plots show that the primary clinopyroxene of sample DHG13 has strong negative anomaly in Ti and low Ti/Eu (856). Other peridotites have high Ti/Eu, >4410. All clinopyroxenes have low LREE/HREE ($(La/Yb)_N < 5$). REE patterns of orthopyroxenes, with positive anomalies in HFSE, show flat HREE to MREE patterns and continuously decreasing normalized abundances from MREE to LREE (Fig. 8b).

6. Discussion

6.1. Early enrichment processes

Clinopyroxene is the major carrier for most trace elements in anhydrous peridotite peridotite, and its trace-element compositions can be used to reveal mantle processes, such as partial melting and metasomatism (Zangana et al., 1999). Recent studies suggested that partition coefficient of REE between orthopyroxene and clinopyroxene (DREE Opx/Cpx) is negatively correlated to cation radius but positively correlated to equilibrium temperature of peridotite (Witt-Eickschen and O'Neill, 2005; Lee et al., 2007). Although the measured partition coefficient of REE between primary clinopyroxene and orthopyroxene broadly increase with decreasing radius (from La to Lu), they are highly variable and do not show positive correlations with equilibrium temperatures (Appendix 2), implying the REE concentrations of primary clinopyroxene are disturbed and can hardly be used to estimate the degree of melt extraction experienced by the studied peridotites.

As no hydrous phases were identified in the studied xenoliths, moderate enrichment of incompatible elements, such as LREE and Sr, is consistent with a cryptic metasomatism. In particular, the convex-upward REE patterns of clinopyroxene, with the peak at Sm, Nd or Eu (Fig. 8a),

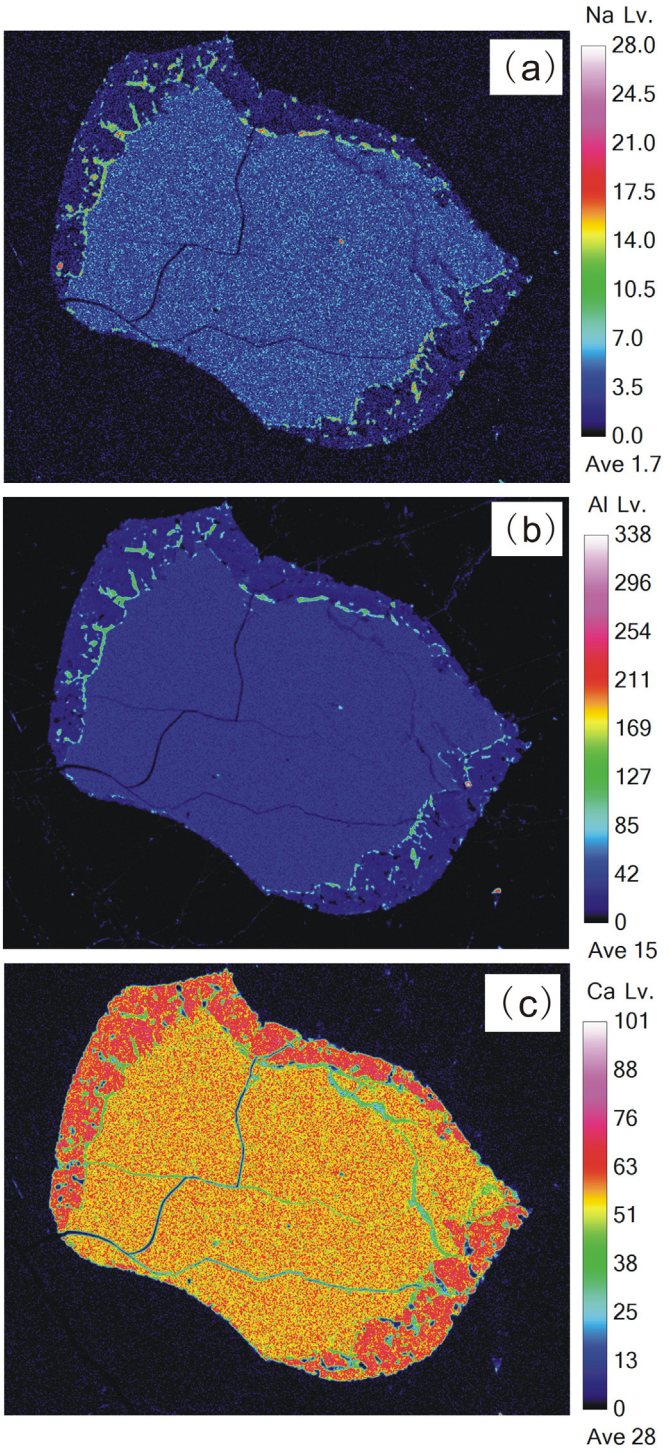

Fig. 7. Compositional mapping of spongy-textured clinopyroxene grain in Fig. 3c. Color bar in the right indicates the relative contents of the selected elements.

are diagnostic of equilibrium with LREE-rich melts (Bodinier et al., 1990; Navon and Stolper 1987). All primary clinopyroxenes, except for those of sample DHG13, with low $(La/Yb)_N$ (< 5) and high Ti/Eu (> 4410), record the signatures of silicate-melt related metasomatism (Coltorti et al., 1999). $Mg^{\#}$ of clinopyroxene in samples AS06 and DHG10 is <89.0, possibly reflecting the addition of iron after partial melting. Clinopyroxene of sample DHG13 has low Ti/Eu of 856 and $(La/Yb)_N$ of 0.23. The patterns are similar to those of clinopyroxene in peridotites from West Tianshan, which have been interpreted to be produced by a metasomatic agent transitional between carbonatitic and silicate melt, or overprinted by multiple episodes of metasomatism (Zheng et al., 2006). Fig. 8a shows that the melts in equilibrium with primary clinopyroxenes had lower REE abundances than the host basalts. We therefore consider that the studied xenoliths had experienced enrichment processes before entrainment.

6.2. Origin of spongy texture in the Aershan peridotites

The origin of spongy texture in mantle clinopyroxene has long been controversial and attributed to interaction between peridotite and host magma (Qi et al., 1995; Shaw et al., 2006; Shaw and Dingwell 2008), decompression-induced melting (Su et al., 2011) and mantle metasomatism by fluid/melt penetration before entrainment (Bonadiman et al., 2005, 2008; Carpenter et al., 2002; Ionov et al., 1994). Based on petrological observations and chemical analysis, decompression-induced partial melting is considered as the most possible mechanism for the formation of spongy texture in the studied peridotites. The evidences are as below:

1. Most studied xenoliths contain symplectite which consists of tiny spinels, orthopyroxenes and quenched glasses. Such symplectites are generally interpreted as the products of breakdown of previous garnet due to pressure decrease (Godard and Martin 2000; Morishita and Arai 2003; Obata 2011; Obata and Ozawa 2011; Špaček et al., 2013). The low CaO content (17.5–20.4 wt%) of the primary clinopyroxene is also considered as reflecting equilibrium with the garnet phase (Bonadiman et al., 2005).

2. Secondary clinopyroxene in spongy domain is characterized by lower Al_2O_3 and Na_2O, but higher CaO, $Cr^{\#}$ and $Mg^{\#}$ than the primary one (Fig. 6). The decrease in Al_2O_3 and increase in $Mg^{\#}$ and $Cr^{\#}$ of clinopyroxene are frequently interpreted as effective indicators of degree of partial melting (e.g. Frey and Prinz 1978; Zheng et al., 2001). Therefore, secondary clinopyroxene in spongy domain could represent residues after partial melting of primary clinopyroxene. The relative proportions of Al^{IV} and Al^{VI} in clinopyroxene can provide useful information on pressure differences (Wass 1979). Primary clinopyroxene (for example, the intact core) has systematically higher Al^{VI}, and more significantly, higher Al^{VI}/Al^{IV} ratios than that of secondary clinopyroxene in spongy domains (1.35–2.57 vs 0.47–1.88, Table 2 and Appendix 1), implying a decompression process. The lower content of Na in secondary clinopyroxene in spongy domains also supports the lower-pressure origin (e.g. Ma et al., 2015).

3. Several thermometers have been adopted to estimate the equilibrium temperatures of the studied peridotites. These thermometers give similar temperatures for each sample (Table 3), with a discrepancy of 3–58 °C, which can generally be reconciled with the uncertainties of used thermometers (for example, 70 °C for Mg-Fe-two-pyroxene thermometer, Wells 1977). Recently, Fan et al., (2008) reported a fresh garnet peridotite xenolith collected near the Chaoer River in the Halaha

Table 3
Estimated temperatures (°C) and pressures (Gpa) for the Aershan peridotites.

Sample	Primary phases				Spongy domain	
	T_{BK-ca}	T_{DE}	T_{Wells}	P	$T_{Putirka-32d}$	$P_{Putirka-32a}$
AS03	1036	1052	1063	2.10	1075	0.95
AS04	1067	1085	1112	2.16	1105	0.57
AS06	1160	1136	1152	2.35	1095	0.58
HLH10	1073	1119	1061	2.18	1098	0.34
DHG04	1173	1201	1181	2.38	1227	0.50
DHG10	1186	1244	1221	2.40	1219	0.49
DHG13	1201	1198	1204	2.44	1127	0.50

T_{BK-Ca}: Ca in Opx thermometer, Brey and Köhler (1990); T_{DE}: Al in Ol thermometer, De Hoog et al. (2010).

T_{Wells}: Mg-Fe-two-pyroxene thermometer, Wells (1977). P for primary phases are estimated from T_{BK-Ca},assuming the studied xenoliths shared the same geothermal gradient with those from Fan et al. (2008).

$P_{Putirka-32a}$ and $P_{Putirka-32d}$: single clinopyroxene thermobarometer, Eqs 32a and 32d from Putirka, (2008).

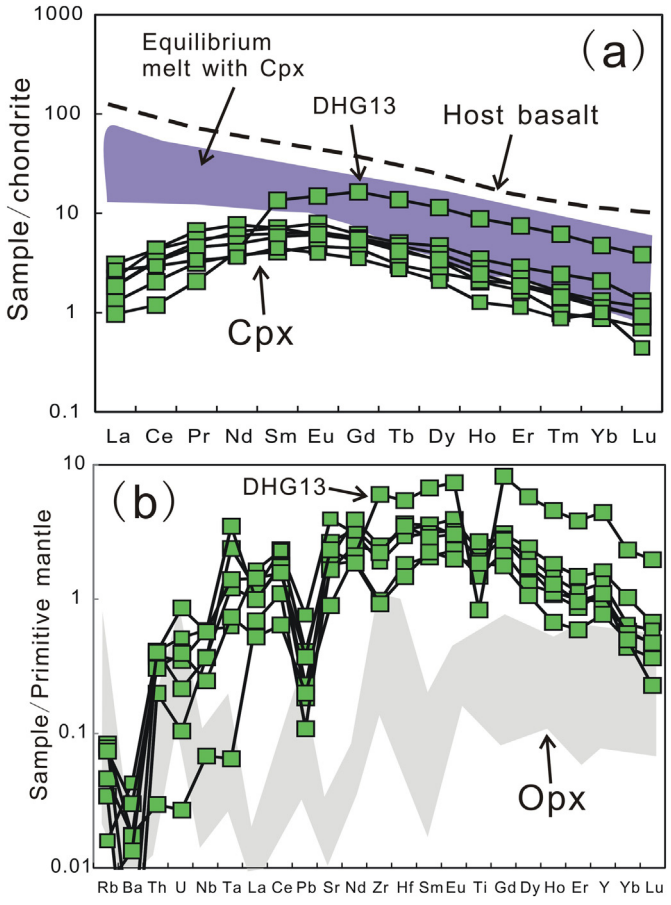

Fig. 8. Chondrite-normalized REE patterns (a) and primitive-mantle-normalized trace-element diagrams for primary clinopyroxenes in the studied xenoliths (b). Melt in equilibrium with primary clinopyroxene was calculated using partition coefficients of Hart and Dunn (1993). Host basalt is from Ho et al. (2013). Normalizing values are from McDonough and Sun (1995).

volcanic field (about 35 km away from our sample location; Fig. 1b), with a temperature-pressure estimate of 1164 °C and 2.36 Gpa. Assuming that the studied xenoliths shared the same geothermal gradient, and accepting their $T_{BK\text{-}Ca}$ (1036–1201 °C) as equilibration temperatures, the pressures of origin would be 2.10–2.44 Gpa. Temperature and pressure for spongy domains can be estimated using the clinopyroxene-only thermobarometer (Eqs 32a and 32d in Putirka 2008), which gives slightly higher temperatures (1175 °C to 1292 °C) but significantly lower pressures (0.34–0.95 Gpa) than those for primary phases. Although pressure estimation for peridotites employing the iterative method of Putirka (2008) carries some uncertainty (Ma et al., 2015) and the estimated pressures for spongy clinopyroxene show large errors (up to 0.6 Gpa), we still suggest that the systematically lower pressures are indicative.

Glasses in spongy domains probably were produced by low-degree melting of primary clinopyroxene. They are rich in Na_2O, SiO_2 and Al_2O_3, similar to low-degree melts obtained by experiments on anhydrous peridotite at pressure of 1.0–1.5 Gpa (Baker et al., 1995; Draper and Green 1997; Robinson et al., 1998). Low-degree melts of anhydrous peridotite at high pressure (e.g. 2.5 Gpa) is characterized by low SiO_2 (e.g. < 50 wt%) and alkali contents because the activity of SiO_2 decreases due to more compatibility of alkali oxide in clinopyroxene at greater depth (Hirschmann et al., 1998; Schiano et al., 2000). Compared with interstitial glasses, melt inclusions in mantle minerals are considered to be preserved in closed systems and devoid of post-entrapment modification. Therefore, homogenized melts inclusions can be used to determine primitive magmas percolating the lithosphere (Bénard et al., 2016; Ionov et al., 2011; Schiano et al., 1998). Glasses studied here have extremely low MgO and FeO contents (both <1 wt%), apparently deviating from the field defined by low-degree melts of anhydrous peridotite and homogenized melt inclusions from Avacha volcano (LD melts and GL-MIs in Fig. 9). The low MgO and FeO contents may be due to crystallization of olivine (presence of olivine traces in spongy domain). More importantly, glasses in some studied xenoliths have low $Mg^{\#}$ (down to 43.8), out of equilibrium with coexisting secondary clinopyroxenes and olivines, assuming the KCpx/lid D Fe/Mg and KOl/lid D Fe/Mg to be 0.28 and 0.30, respectively (Putirka 2008). The lack of equilibrium, combined with ubiquitous presence of glasses, implies that the spongy texture was formed quickly and recently. The decompression event possibly was related to the tectonic extension which resulted in the eruption of the widely distributed Cenozoic alkali basalts across the NE China (e.g. the host magma). Since Late Cretaceous time, the NE China has experienced a period of magmatic relaxation until the eruption of the basalts (Zhang et al., 2000).

6.3. Differentiating various origins of spongy texture in mantle clinopyroxene

As mentioned above, three processes have been considered to be responsible for the formation of spongy texture in mantle clinopyroxene, including interaction between peridotite and host magma (Shaw et al., 2006; Shaw and Dingwell 2008); metasomatism by fluid/melt penetration (Bonadiman et al., 2005); decompression-induced melting (Su et al., 2011; this study). Here, we have summarized the petrologic and chemical differences of spongy-textured clinopyroxene formed by the three processes (Table 4). The comparison allows us to establish textural and chemical criteria to identify the origins of these similar spongy textures in mantle clinopyroxene.

1. Petrologic differences: The interaction between orthopyroxene and host magma during transport could produce a Si- and alkali-rich melt, which is a necessary precursor to formation of spongy texture in clinopyroxene (Shaw et al., 2006; Shaw and Dingwell 2008). In those studies, spongy-textured clinopyroxene, as well as reacted orthopyroxene, is particularly concentrated near contacts with the host magma (Shaw et al., 2006; Shaw and Dingwell 2008). In contrast, orthopyroxenes in peridotites studied here are generally well-preserved (Appendix 3). Spongy-textured clinopyroxenes are randomly distributed in the thin section and do not exhibit preferential development toward the contacts between peridotite and host basalts (Fig. 2). This is consistent with peridotite xenoliths from the Western Qinling area, in which the spongy texture was interpreted as products of decompression-induced melting of clinopyroxene (Su et al., 2011). Peridotite xenoliths from Sal Island contain spongy-textured clinopyroxenes, which are accompanied with abundant melt pockets, interstitial glasses and modal metasomatic minerals (Bonadiman et al., 2005; Ionov et al. 2005). Kimberlite-like melt infiltration was considered as the mechanism responsible for the spongy texture (Bonadiman et al., 2005). All peridotites studied here are anhydrous and contain no modal metasomatic phases. Spongy domains do not appear to preferentially develop along cracks cross clinopyroxenes (Fig. 3c). These features argue against the infiltration of melt/fluid. Although melt pockets were observed in peridotites from the West Qinling area, the authors interpreted those melt pockets as formed after spongy clinopyroxene (Su et al., 2010).

2. Chemical differences: Secondary clinopyroxene in spongy domain has lower Al_2O_3 and Na_2O, but higher CaO, $Cr^{\#}$ and $Mg^{\#}$, than the primary one, regardless of the interpreted origin (Figs. 6). Their plotted areas overlap with each other, and therefore cannot be used to constrain the origin of spongy clinopyroxene. Glasses are commonly observed associated with spongy-textured clinopyroxene (Bonadiman et al., 2005; Carpenter et al., 2002; Ionov et al., 2005; Shaw et al., 2006). They have different major-oxide contents which can be used to differentiate the origins of spongy texture in mantle clinopyroxene. Glasses within spongy domains studied here (decompression-induced melting of

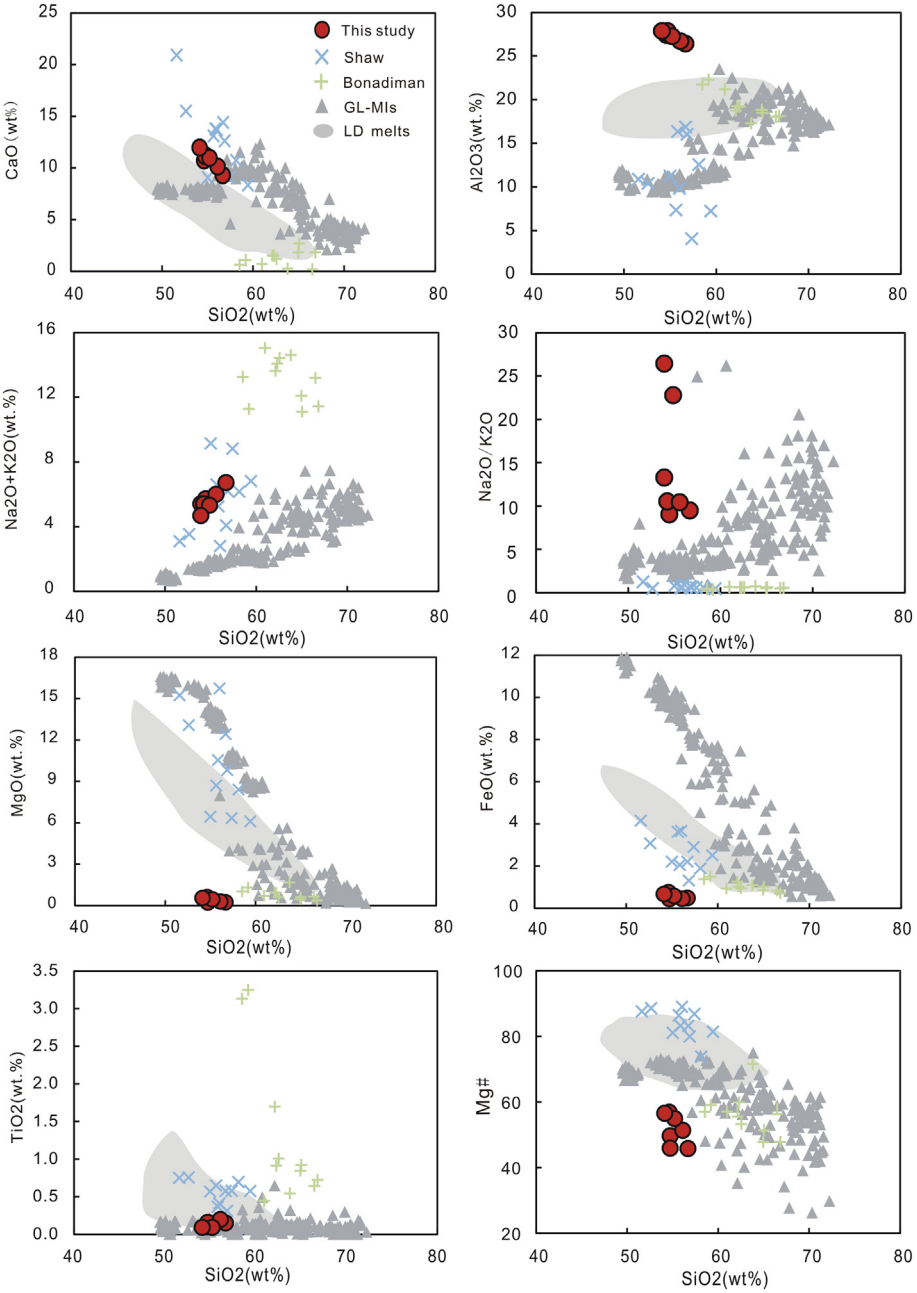

Fig. 9. Plots (recalculated on an anhydrous basis) of SiO_2 vs (a) CaO, (b) Al_2O_3, (c) $Na_2O + K_2O$ (d) Na_2O/K_2O, (e) MgO, (f) FeO, (g) TiO_2 and (h) $Mg^{\#}$ in glasses associated with spongy clinopyroxene of various origins. Shaw and Bonadiman: glass associated with spongy-texture clinopyroxene; GL-MIs: homogenized (heated) glass inclusions from subduction zones; LD melts: low-degree melts produced by experiments on anhydrous peridotite. Data sources: Shaw are from Shaw et al. (2006) and Shaw and Dingwell (2008); Bonadiman are from Bonadiman et al. (2005); GL-MIs are from Ionov et al. (2011) and Bénard et al. (2016); LD melts are from Baker et al., (1995), Draper and Green. (1997) and Robinson et al. (1998). Note K_2O contents of LD melts are generally not reported.

clinopyroxene) show narrow ranges of major-element compositions (Fig. 9). They have obviously higher Al_2O_3 (26.4–27.8 wt%) and Na_2O/K_2O (up to 26.4), compared with those related to spongy textures of other origins (Shaw and Bonadiman in Fig. 9). The Al_2O_3 contents of the studied glasses are even higher than those of low-degree melts of anhydrous peridotites and most Al-rich primitive melts percolating the lithosphere (LD melts and GL-MIs in Fig. 9). Glasses in peridotites from Sal Island (metasomatism by melt infiltration, Bonadiman in Fig. 9) contain large amounts of Na_2O and K_2O (up to 15 wt%) and have low CaO (< 3 wt%) and Na_2O/K_2O (< 1), which cannot be produced by melting of clinopyroxene and exotic alkali-rich agent must be evoked. Strong penetration of kimberlite-like melt was considered as the mechanism responsible for the formation of spongy texture (Bonadiman et al., 2005). Glasses within spongy-textured clinopyroxene, which were formed by host magma-peridotite interaction (Shaw in Fig. 9), are characterized by high MgO and FeO, as well as $Mg^{\#}$. They also have low Na_2O/K_2O, due to the involvement of alkali-rich melts released by dissolution of orthopyroxene (Shaw et al., 2006; Shaw and Dingwell 2008).

7. Concluding remarks

1. The peridotite xenoliths from the eastern Central Asian Orogenic Belt contain spongy-textured clinopyroxene. The spongy domains are variable in thickness and consists of clinopyroxenes, glasses, vugs and traces of olivine.

Table 4
Petrologic and geochemical differences of spongy texture in mantle clinopyroxene with various origins.

Origin	Petrologic differences	Chemical differences (associated glasses)	References
Decompression-induced partial melting	No melt pocket or modal metasomatic mineral; no preferential development of spongy texture toward host magma and along cracks; orthopyroxene well preserved	High Al_2O_3 and Na_2O/K_2O; low MgO, FeO and $Mg^{\#}$	This study
Host lava-peridotite interaction	Presence of reacted orthopyroxene; preferential development of spongy texture toward host magma	High MgO, FeO and $Mg^{\#}$; low Na_2O/K_2O	Shaw et al. 2006; Shaw and Dingwell 2008
Metasomatism by melt infiltration	Presence of melt pockets, glass patches and modal metasomatic minerals	High $Na_2O + K_2O$; low CaO and Na_2O/K_2O	Bonadiman et al. 2005

2. Spongy texture in the studied peridotites was formed by decompression-induced melting of clinopyroxene.

3. The differences in petrologic characteristics and major-element compositions of associated glasses can be used to identify origin of spongy texture in mantle clinopyroxene.

Acknowledgements

We specially thank two reviewers for their constructive comments. We also thank Dr. Xianhua Li and Ms. Rohini Shivaram for editorial handling. The research was financially supported by National Nature Science Foundation of China (No. 41402049), The DREAM project of MOST, China (NO. 2016YFC0600403) and the Fundamental Research Funds for the Central Universities (No. G1323527688). This is contribution 1201 from the ARC Centre of Excellence for Core to Crust Fluid Systems (www.ccfs.mq.edu.au) and 1251 from the GEMOC Key Centre (www.gemoc.mq.edu.au).

Appendix A. Supplementary data

Supplementary data to this article can be found online at https://doi.org/10.1016/j.lithos.2018.08.035.

References

Baker, M.B., Hirschmann, M.M., Ghiorso, M.S., Stolper, E.M., 1995. Compositions of near-solidus peridotite melts from experiments and thermodynamic calculations. Nature 375, 308–311.

Bénard, A., Nebel, O., Ionov, D.A., Arculus, R.J., Shimizu, N., Métrich, N., 2016. Primary silica-rich picrite and high-ca boninite melt inclusions in pyroxenite veins from the Kamchatka sub-arc mantle. Journal of Petrology 57, 1959–1982.

Bodinier, J.L., Vasseur, G., Vernieres, J., Dupuy, C., Fabries, J., 1990. Mechanisms of mantle metasomatism: geochemical evidence from the Lherz orogenic peridotite. Journal of Petrology 31, 597–628.

Bonadiman, C., Coltorti, M., Beccaluva, L., Siena, F., 2005. Kimberlite-like Metasomatism and 'Garnet Signature' in Spinel-peridotite Xenoliths from Sal, Cape Verde Archipelago: Relics of a Subcontinental Mantle Domain within the Atlantic Oceanic Lithosphere? Journal of Petrology 46, 2465–2493.

Bonadiman, C., Coltorti, M., Beccaluva, L., Siena, F., 2008. Mantle Metasomatism *vs.* Host Magma Interaction: The Ongoing Controversy. Geophysical Research Abstracts 10. EGU2008-A-09723.

Brey, G.P., Köhler, T., 1990. Geothermobarometry in four-phase lherzolites II. New thermobarometers, and practical assessment of existing thermobarometers. Journal of Petrology 31, 1353–1378.

Carpenter, R.L., Edgar, A.D., Thibault, Y., 2002. Origin of spongy textures in clinopyroxene and spinel from mantle xenoliths, Hessian Depression, Germany. Mineralogy and Petrology 74, 149–162.

Coltorti, M., Bonadiman, C., Hinton, R.W., Siena, F., Upton, B.G.J., 1999. Carbonatite metasomatism of the oceanic upper mantle: evidence from clinopyroxenes and glasses in ultramafic xenoliths of Grande Comore, Indian Ocean. Journal of Petrology 40, 133–165.

Dawson, J.B., 2002. Metasomatism and partial melting in upper-mantle peridotite xenoliths from the Lashaine volcano, Northern Tanzania. Journal of Petrology 43, 1749–1777.

De Hoog, J., Gall, L., Cornell, D.H., 2010. Trace-element geochemistry of mantle olivine and application to mantle petrogenesis and geothermobarometry. Chemical Geology 270, 196–215.

Draper, D.S., Green, T.H., 1997. P-T phase relations of silicic, alkaline, aluminous mantle xenolith glasses under anhydrous and C-O-H fluid-saturated conditions. Journal of Petrology 38, 1187–1224.

Fan, Q.C., Sui, J.L., Zhao, Y.W., Sun, Q., Li, N., Du, X.X., 2008. Preliminary study on garnet peridotite xenoliths of Quaternary volcanic rocks in middle Daxing'an Mountain Range. Acta Petrologica Sinica 24, 2563–2568 (in Chinese with English abstract).

Frey, F.A., Prinz, M., 1978. Ultramafic inclusions from San Carlos, Arizona: petrologic and geochemical data bearing on their petrogenesis. Earth and Planetary Science Letters 38, 129–176.

Ge, W.C., Wu, F.Y., Zhou, C.Y., Abdel Rahman, A.A., 2005. Emplacement age of the Tahe granite and its constraints on the tectonic nature of the Erguna block in the northern part of the Da Hinggan Range. Chinese Science Bulletin 50, 2097–2105.

Ge, M.C., Zhou, W.X., Yu, Y., Sun, J.J., Bao, J.Q., Wang, S.H., 2011. Dissolution and supracrustal rocks dating of Xilin Gol complex, Inner Mongolia, China. Earth Science Frontiers 18, 182–195 (in Chinese with English abstract).

Godard, G., Martin, S., 2000. Petrogenesis of kelyphites in garnet peridotites: a case study from the Ulten zone, Italian Alps. Journal of Geodynamics 30, 117–145.

Griffin, W.L., Zhang, A.D., O Reilly, S.Y., Ryan, C.G., 1998. Phanerozoic Evolution of the Lithosphere beneath the Sino-Korean Craton. In: Flower, M., Chung, S.L., Lo, C.H., Lee, T.Y. (Eds.), Mantle Dynamics and Plate Interactions in East Asia. American Geophysical Union Vol. 27, pp. 107–126.

Hart, S.R., Dunn, T., 1993. Experimental cpx/melt partitioning of 24 trace elements. Contributions to Mineralogy and Petrology 113, 1–8.

Hirschmann, M.M., Baker, B., Stolper, E.M., 1998. The effect of alkalis on the silica content of mantle-derived melts. Geochimica et Cosmochimica Acta 62, 883–902.

Ho, K.S., Ge, W.C., Chen, J.C., You, C.F., Yang, H.R., Zhang, Y.L., 2013. Late Cenozoic magmatic transitions in the central Great Xing'an Range, Northeast China: Geochemical and isotopic constraints on petrogenesis. Chemical Geology 352, 1–18.

Ionov, D.A., Hofmann, N.W., Shimiru, N., 1994. Metasomatism-induced melting in mantle xenoliths from Mongolia. Journal of Petrology 35, 753–785.

Ionov, D.A., Prikhodko, V.S., Bodinier, J.L., Sobolev, A.V., Weis, D., 2005. Lithospheric mantle beneath the south-eastern Siberian craton: petrology of peridotite xenoliths in basalts from the Tokinsky Stanovik. Contributions to Mineralogy and Petrology 149, 647–665.

Ionov, D.A., Bénard, A., Plechov, P.Y., 2011. Melt evolution in sub-arc mantle: evidence from heating experiments on melt inclusions in peridotite xenoliths from the andesitic Avacha volcano (Kamchatka, Russia). Contributions to Mineralogy and Petrology 162, 1159–1174.

Jahn, B., Wu, F., Chen, B., 2000. Massive granitoid generation in Central Asia: Nd isotope evidence and implication for continental growth in the Phanerozoic. Episodes 23, 82–92.

Kaeser, B., Kalt, A., Pettke, T., 2007. Crystallization and breakdown of metasomatic phases in graphite-bearing peridotite xenoliths from Marsabit (Kenya). Journal of Petrology 48, 1725–1760.

Kröner, A., Windley, B.F., Badarch, G., Tomurtogoo, O., Hegner, E., Jahn, B.M., Gruschka, S., Khain, E.V., Demoux, A., Wingate, M., 2007. Accretionary growth and crust formation in the Central Asian Orogenic Belt and comparison with the Arabian-Nubian shield. Geological Society of America Memoirs 200, 181–209.

Liang, Y., Elthon, D., 1990. Geochemistry and petrology of spinel lherzolite xenoliths from Xalapasco de La Joya, San Luis Potosi, Mexico: partial melting and mantle metasomatism. Journal of Geophysical Research B95, 15859–15877.

Liu, Y.S., Hu, Z.C., Gao, S., Günther, D., Xu, J., Gao, C., Chen, H.H., 2008. In situ analysis of major and trace elements of anhydrous minerals by LA-ICP-MS without applying an internal standard. Chemical Geology 257, 34–43.

Liu, J.L., Wang, J., Song, Y., Liu, J.G., Li, A., 2014. Study on SCLM in Aershan-Chaihe area of Inner Mongolia: evidence from trace elements of clinopyroxene. Global Geology 33, 1–10 (in Chinese with English abstract).

Ma, G.S.K., Wang, K.L., Malpas, J., Iizuka, Y., Xenophontos, C., Turkmani, A.A., Chan, G.H.N., Usuki, T., Chan, Q.H.S., 2015. In: Khan, A., Deschamps, F. (Eds.), Melt Pockets and Spongy Clinopyroxenes in Mantle Xenoliths from the Plio-Quaternary Al Ghab Volcanic Field, NW Syria: Implications for the Metasomatic Evolution of the Lithosphere. Springer Geophysics, pp. 205–258 The Earth's Heterogeneous Mantle: A Geophysical, Geodynamical and Geochemical Perspective.

McDonough, W.F., Sun, S.S., 1995. The composition of the Earth. Chemical Geology 120, 223–253.

Miao, L.C., Fan, W.M., Zhang, F.Q., Liu, D.Y., Jian, P., Shi, G.H., Tao, H., Shi, Y.R., 2004. Zircon SHRIMP geochronology of the Xinkailing–Kele complex in the northwestern Lesser Xing'an Range, and its geological implications. Chinese Science Bulletin 49, 201–209.

Morishita, M., Arai, S., 2003. Evolution of spinel-pyroxene symplectite in spinel–lherzolites from the Horoman complex, Japan. Contributions to Mineralogy and Petrology 144, 509–522.

Navon, O., Stolper, E., 1987. Geochemical consequences of melt percolation: the uppermantle as a chromatographic column. Journal of Geology 95, 285–307.

Nelson, S.T., Montana, A., 1992. Sieve-textured plagioclase in volcanic rocks produced by rapid decompression. American Mineralogist 77, 1242–1249.

Obata, M., 2011. Kelyphite and Symplectite: Textural and Mineralogical Diversities and Universality, and a New Dynamic View of their Structural Formation. In: Sharkov, E. V. (Ed.), New Frontiers in Tectonic Research-General Problems, Sedimentary Basins and Island Arcs. Rijeka. InTech, pp. 93–122.
Obata, M., Ozawa, K., 2011. Topotaxic relationships between spinel and pyroxene in kelzphite after garnet in mantle-derived peridotites and their implications to reaction mechanism and kinetics. Mineralogy and Petrology 101, 217–224.
Pan, S.K., Zheng, J.P., Griffin, W.L., Chu, L.L., 2013. Coexistence of the moderately refractory and fertile lithospheric mantle beneath the eastern Central Asian Orogenic Belt. Gondwana Research 23, 176–189.
Pan, S.K., Zheng, J.P., Griffin, W.L., Chu, L.L., Xu, Y.X., Li, Y.L., Ma, Q., Wang, D., 2014. Precambrian tectonic attribution and evolution of the Songliao terrane revealed by zircon xenocrysts from Cenozoic alkali basalts, Xilinhot region, NE China. Precambrian Research 251, 33–48.
Pan, S.K., Zheng, J.P., Griffin, W.L., Xu, Y.X., Li, X.Y., 2015. Nature and evolution of the lithospheric mantle beneath the eastern Central Asian Orogenic Belt: constraints from peridotite xenoliths in the central part of the Great Xing'an Range, NE China. Lithos 238, 52–63.
Putirka, K.D., 2008. Thermometers and Barometers for Volcanic Systems. Reviews in Mineralogy and Geochemistry 69, 61–120.
Qi, Q., Taylor, L.A., Zhou, X.M., 1995. Petrology and geochemistry of mantle peridotite xenoliths from SE China. Journal of Petrology 36, 55–79.
Robinson, J.A.C., Wood, B.J., Blundy, J.D., 1998. The beginning of melting of fertile and depleted peridotite at 1.5 GPa. Earth and Planetary Science Letters 155, 97–111.
Schiano, P., Bourdon, B., Clocchiatti, R., Massare, D., Varela, M.E., Bottinga, Y., 1998. Low-degree partial melting trends recorded in upper mantle minerals. Earth and Planetary Science Letters 160, 500–537.
Schiano, P., Clocchiatti, R., Bourdon, B., Burton, K.W., Thellier, B., 2000. The composition of melt inclusions in minerals at the garnet-spinel transition zone. Earth and Planetary Science Letters 174, 375–383.
Sengör, A., Burtman, V.S., 1993. Evolution of the Altaid tectonic collage and Palaeozoic crustal growth in Eurasia. Nature 364, 299–307.
Shaw, C.S.J., Dingwell, D.B., 2008. Experimental peridotite–melt reaction at one atmosphere: a textural and chemical study. Contributions to Mineralogy and Petrology 155, 199–214.
Shaw, C.S.J., Heidelbach, F., Dingwell, D.B., 2006. The origin of reaction textures in mantle peridotite xenoliths from Sal Island, Cape Verde: the case for "metasomatism" by the host lava. Contributions to Mineralogy and Petrology 151, 681–697.
Shi, G.H., Liu, D.Y., Zhang, F.Q., Jian, P., Miao, L.C., Shi, Y.R., Tao, H., 2003. Zircon SHRIMP U–Pb geochronology and significance of the Xilinhot metamorphic complex, Inner Mongolia. China. Chinese Science Bulletin 48, 2742–2748.
Špaček, P., Ackerman, M., Habler, G., Abart, R., Ulrych, J., 2013. Garnet Breakdown, Symplectite Formation and Melting in Basanite-hosted Peridotite Xenoliths from Zinst (Bavaria, Bohemian Massif). Journal of Petrology 54, 1691–1723.
Streck, M.J., 2008. Mineral textures and zoning as evidence for open system processes. Reviews in Mineralogy and Geochemistry 69, 595–622.
Su, B.X., Zhang, H.F., Patrick, A.S., Qin, K.Z., Liu, P.P., Ying, J.F., Tang, Y.J., Sanjeewa, P.K.M., Xiao, Y., Zhao, X.M., Mao, Q., Ma, Y.G., 2010. Formation of melt pocket in mantle peridotite xenolith from western Qinling, Central China: Partial melting and metasomatism. Journal of Earth Science 21, 641–668.
Su, B.X., Zhang, H.F., Sakyi, P.A., Zhang, Y.H., Ying, J.F., Tang, Y.J., Qin, K.Z., Xiao, Y., Zhao, X. M., Mao, Q., Ma, Y.G., 2011. The origin of spongy texture in minerals of mantle xenoliths from the Western Qinling, Central China. Contributions to Mineralogy and Petrology 161, 465–482.
Sun, L.X., Ren, B.F., Zhao, F.Q., Gu, Y.C., Li, Y.F., Liu, H., 2013a. Zircon U-Pb dating and Hf isotopic compositions of the Mesoporterozoic granitic gneiss in Xilinhot Block, Inner Mongolia. Geological Bulletin of China 32 (2–3), 327–340 (in Chinese with English abstract).
Sun, L.X., Ren, B.F., Zhao, F.Q., Ji, S.P., Geng, J.Z., 2013b. Late Paleoproterozoic magmatic records in the Eerguna massif: evidences from the zircon U-Pb dating of granitic gneisses. Geological Bulletin of China 32, 341–352 (in Chinese with English abstract).
Tang, Y.J., Zhang, H.F., Ying, J.F., Su, B.X., 2013a. Widespread refertilization of cratonic and circum-cratonic lithospheric mantle. Earth-Science Reviews 118, 45–68.
Tang, J., Xu, W.L., Wang, F., Wang, W., Xu, M.J., Zhang, Y.H., 2013b. Geochronology and geochemistry of Neoproterozoic magmatism in the Erguna Massif, NE China: Petrogenesis and implications for the breakup of the Rodinia supercontinent. Precambrian Research 224, 597–611.
Tang, J., Xu, W.L., Wang, F., Wang, W., Xu, M.J., Zhang, Y.H., 2014. Geochronology and geochemistry of early-middle Triassic magmatism in the Erguna Massif, NE China: constraints on the tectonic evolution of the Mongol-Okhotsk suture belt. Lithos 184, 187, 1–16.
Thompson, R.N., Gibson, S.A., 2000. Transient high temperatures in mantle plume heads inferred from magnesian olivines in Phanerozoic picrites. Nature 407, 502–506.
Wang, F., Zhou, X.H., Zhang, L.C., Ying, J.F., Zhang, Y.T., Wu, F.Y., Zhu, R.X., 2006. Late Mesozoic volcanism in the Great Xing'an Range (NE China): timing and implications for the dynamic setting of NE Asia. Earth and Planetary Science Letters 251, 179–198.
Wass, S., 1979. Multiple origins of clinopyroxenes in alkali basaltic rocks. Lithos 12, 115–132.
Wells, P., 1977. Pyroxene thermometry in simple and complex systems. Contributions to Mineralogy and Petrology 62, 129–139.
Wilhem, C., Windley, B.F., Stampfli, G.M., 2012. The Altaids of Central Asia: a tectonic and evolutionary innovative review. Earth-Science Reviews 113, 303–341.
Windley, B.F., Alexeiev, D., Xiao, W., Kröner, A., Badarch, G., 2007. Tectonic models for accretion of the Central Asian Orogenic Belt. Journal of the Geological Society 164, 31–47.
Wu, F.Y., Sun, D.Y., Li, H.M., Wang, X., 2001. The nature of basement beneath the Songliao Basin in NE China: geochemical and isotopic constraints. Physics and Chemistry of the Earth, Part A: Solid Earth and Geodesy 26, 793–803.
Wu, F.Y., Sun, D.Y., Li, H.M., Jahn, B., Wilde, S.A., 2002. A-type granites in northeastern China: age and geochemical constraints on their petrogenesis. Chemical Geology 187, 143–173.
Wu, F.Y., Walker, R.J., Ren, X., Sun, D., Zhou, X., 2003. Osmium isotopic constraints on the age of lithospheric mantle beneath northeastern China. Chemical Geology 196, 107–129.
Wu, F.Y., Sun, D.Y., Ge, W.C., Zhang, Y.B., Grant, M.L., Wilde, S.A., Jahn, B., 2011. Geochronology of the Phanerozoic granitoids in northeastern China. Journal of Asian Earth Sciences 41, 1–30.
Xiao, W.J., Windley, B.F., Hao, J., Zhai, M.G., 2003. Accretion leading to collision and the Permian Solonker suture, Inner Mongolia, China: termination of the central Asian orogenic belt. Tectonics 22, 1069–1089.
Xu, Y.G., Menzies, M.A., Vroon, P., Mercier, J.C., Lin, C.Y., 1998. Texture-temperature-geochemistry relationships in the upper mantle as revealed from spinel peridotite xenoliths from Wangqing, NE China. Journal of Petrology 39, 469–493.
Xu, Y.G., Chung, S.L., Ma, J.L., Shi, L.B., 2004. Contrasting Cenozoic lithospheric evolution and architecture in the western and eastern Sino-Korean Craton: constraints from geochemistry of basalts and mantle xenoliths. Journal of Geology 112, 593–605.
Xu, W.L., Pei, F.P., Wang, F., Meng, E., Ji, W.Q., Yang, D.B., Wang, W., 2013. Spatial-temporal relationships of Mesozoic volcanic rocks in NE China: constraints on tectonic overprinting and transformations between multiple tectonic regimes. Journal of Asian Earth Science 74, 167–193.
Yu, S.Y., Xu, Y.G., Huang, X.L., Ge, W.C., Ma, J.L., 2007. Characteristics of melt-rock reaction in Shuangliao peridotite xenoliths and their implications to mantle metasomatism. Acta Petrologica et Mineralogica 26, 213–222 (in Chinese with English abstract).
Yu, S.Y., Xu, Y.G., Huang, X.L., Ma, J.L., Ge, W.C., Zhang, H.H., Qin, X.F., 2009. Hf-Nd isotopic decoupling in continental mantle lithosphere beneath Northeast China: Effects of pervasive mantle metasomatism. Journal of Asian Earth Sciences 35, 554–570.
Zangana, N.A., Downes, H., Thirlwall, M.F., Marriner, G.F., Bea, F., 1999. Geochemical variation in peridotite xenoliths and their constituent clinopyroxenes from Ray Pic (French Massif Central): implications for the composition of the shallow lithospheric mantle. Chemical Geology 153, 11–35.
Zhang, R.X., Yang, S.Y., 2016. A mathematical model for determining carbon coating thickness and its application in electron probe microanalysis. Microscopy and Microanalysis 22, 1374–1380.
Zhang, M., Suddaby, P., O'Reilly, S.Y., Norman, M., Qiu, J., 2000. Nature of the lithospheric mantle beneath the eastern part of the Central Asian fold belt: mantle xenolith evidence. Tectonophysics 328, 131–156.
Zhang, J.H., Gao, S., Ge, W.C., Wu, F.Y., Yang, J., Wilde, S.A., Li, M., 2010. Geochronologyof the Mesozoic volcanic rocks in the Great Xing'an Range, northeastern China: implications for subduction-induced delamination. Chemical Geology 276, 144–165.
Zhang, Y.L., Liu, C.Z., Ge, W.C., Wu, F.Y., Chu, Z.L., 2011. Ancient sub-continental lithospheric mantle (SCLM) beneath the eastern part of the Central Asian Orogenic Belt (CAOB): implications for crust–mantle decoupling. Lithos 126, 233–247.
Zhang, M., Yang, J.H., Sun, J.F., Wu, F.Y., Zhang, M., 2012. Juvenile subcontinental lithospheric mantle beneath the eastern part of the Central Asian Orogenic Belt. Chemical Geology 328, 109–122.
Zheng, J.P., O'Reilly, S.Y., Griffin, W.L., Lu, F.X., Zhang, M., Pearson, N.J., 2001. Relict refractory mantle beneath the eastern North China block: significance for lithosphere evolution. Lithos 57, 43–66.
Zheng, J.P., Griffin, W.L., O'Reilly, S.Y., Zhang, M., Person, N., Luo, Z.H., 2006. The lithospheric mantle beneath the southwestern Tianshan area, northwest China. Contributions to Mineralogy and Petrology 151, 451–479.
Zheng, J.P., Griffin, W.L., O'Reilly, S.Y., Yu, C.M., Zhang, H.F., Pearson, N., Zhang, M., 2007. Mechanism and timing of lithospheric modification and replacement beneath the eastern North China Craton: peridotitic xenoliths from the 100 Ma Fuxin basalts and a regional synthesis. Geochimica et Cosmochimica Acta 71, 5203–5225.
Zheng, J.P., 2009. Comparison of mantle-derived matierals from different spatiotemporal settings: Implications for destructive and accretional processes of the North China Craton. Chinese Science Bulletin 54, 3397–3416.
Zhou, Q., Wu, F.Y., Chu, Z.Y., Yang, Y.H., Sun, D.Y., Ge, W.C., 2007. Sr-Nd-Hf-Os isotopic characterizitions of the Jiaohe peridotite xenoliths in Jilin province and constraints on the lithospheric mantle age in northeastern China. Acta Petrologica Sinica 23, 1269–1280 (in Chinese with English abstract).
Zhou, Q., Wu, F.Y., Chu, Z.Y., Ge, W.C., 2009. Isotopic compositions of mantle xenoliths and age of the lithospheric mantle in Yition, Jilin Province. Acta Petrologica Sinica 26, 1241–1264 (in Chinese with English abstract).